# Isogeometric analysis of planar curved Euler-Bernoulli beams having large displacements and small strains

Hokkaido University ○ Student Member Nghi Huu DUONG
Thammasat University
Duy Tan University Duy VO
Thammasat University Pruettha NANAKORN
Hokkaido University Member Takashi MATSUMOTO

## 1. INTRODUCTION

Isogeometric analysis (IGA) has been gaining popularity due to the accuracy and flexibility of its approximation schemes by using different computer-aided design (CAD) splines, i.e., T-splines, U-splines, S-splines, and B-splines. The IGA approach has been appropriately used to analyze various computational mechanics problems, including beam structures having large displacements. Based on the IGA concept, a planar straight Euler-Bernoulli beam element is introduced in [1], in which rational Bézier curves are used. In addition, a planar straight Timoshenko beam element is developed in [2] using B-splines. These straight elements are developed under the assumption of small strains. The assumption of small strains simplifies the formulations but still preserves their efficiency and accuracy. Planar curved Euler-Bernoulli and planar curved Timoshenko beam elements are introduced by the same group of authors in [3, 4]. The most popular IGA approximation scheme using non-uniform rational B-splines (NURBS) is employed in these curved beam elements. Under curvilinear coordinate systems, these curved beam elements are suitable for beam structures having large deformations and complex geometry. They also require much smaller numbers of degrees of freedom (DOFs) than those of straight elements.

By considering the advantages of the studies mentioned above, a planar straight beam element for large displacement analysis is introduced in this paper. Here, the Euler-Bernoulli beam theory and the total Lagrangian formulation are applied. The proposed element is developed under a curvilinear coordinate system to create flexible applications. In addition, the assumption of small strains is also adopted. The kinematic variables are approximated by rational cubic Bézier curves. The validity of the proposed element is demonstrated by solving a problem of a deep circular arch subjected to a concentrated force at its apex. Good numerical results in this study demonstrate the applicability of the element to solving planar curved beam problems with complex deformations.

## 2. KINEMATICS OF A CURVED EULER-BERNOULLI BEAM

### 2.1. Strain and stress measures

The kinematics of a curved Euler-Bernoulli beam under a curvilinear coordinate system is shown in Fig 1. The definitions of $\mathbf{A}_1$, $\mathbf{A}_2$, $\mathbf{G}_1$, $\mathbf{G}_2$, $\mathbf{a}_1$, $\mathbf{a}_2$, $\mathbf{g}_1$, $\mathbf{g}_2$ can be found in [3]. The covariant vectors $\mathbf{G}_1$ and $\mathbf{G}_2$ is employed as the basis vectors of the curvilinear coordinate system in the reference configuration. Their reciprocal contravariant basis vectors are denoted by $\mathbf{G}^1$ and $\mathbf{G}^2$ and defined as [3]

$$\mathbf{G}_\alpha . \mathbf{G}^\beta = \begin{cases} 0 & \alpha \neq \beta \\ 1 & \alpha = \beta \end{cases} \quad (1)$$

where $\alpha, \beta = 1,2$.

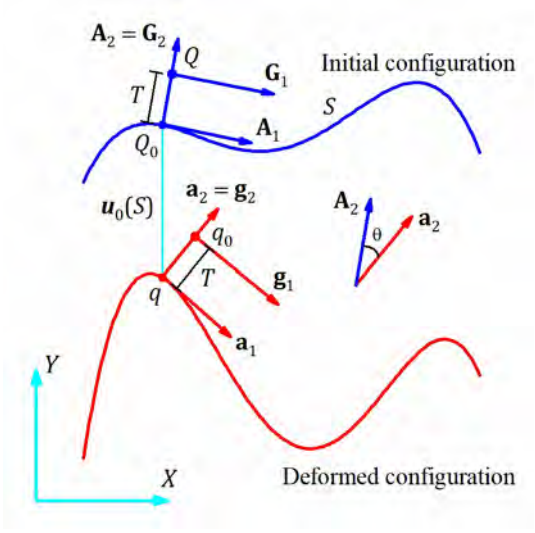


Fig 1. Kinematics of a curved Euler-Bernoulli beam

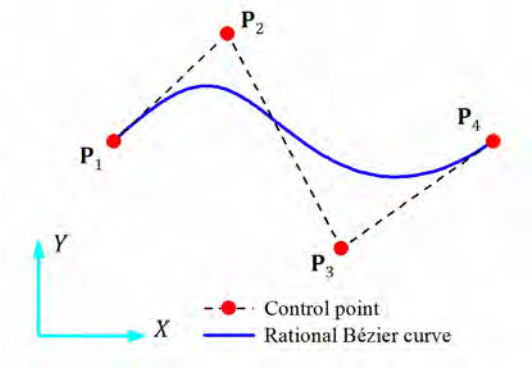


Fig 2. A rational cubic Bézier curve



 

The Green-Lagrange strain tensor $\mathbf{E}$ is measured in the contravariant curvilinear coordinate system $\mathbf{G}^{\alpha} \otimes \mathbf{G}^{\beta}$ as [3]

$$\mathbf{E} = \frac{1}{2}(\mathbf{F}^{\mathrm{T}}\mathbf{F} - \mathbf{G}) \tag{2}$$

where $\mathbf{F} = \mathbf{g}_{\alpha} \otimes \mathbf{G}^{\alpha}$ is the deformation gradient tensor and $\mathbf{G} = G_{\alpha\beta}\mathbf{G}^{\alpha} \otimes \mathbf{G}^{\beta}$ is the metric tensor defined in the reference configuration.

With $\theta$ taken as the smaller angle between the vectors $\mathbf{A}_2$ and $\mathbf{a}_2$, the right stretch tensor $\mathbf{U}$ and the transpose of the rotation matrix $\mathbf{\Lambda}^{\mathrm{T}}(\theta)$ are written as

$$\mathbf{U} = \mathbf{\Lambda}^{\mathrm{T}}(\theta)\mathbf{F} \tag{3}$$

$$\begin{aligned} \mathbf{\Lambda}^{\mathrm{T}}(\theta) &= \mathbf{A}_1 \otimes \frac{\mathbf{a}_1}{a_1} + \mathbf{A}_2 \otimes \mathbf{a}_2 \\ &= \frac{\mathbf{G}_1}{G_1} \otimes \frac{\mathbf{g}_1}{g_1} + \mathbf{G}_2 \otimes \mathbf{g}_2 \end{aligned} \tag{4}$$

where $a_1$, $g_1$ and $G_1$ are the lengths of vectors $\mathbf{a}_1$, $\mathbf{g}_1$ and $\mathbf{G}_1$, respectively.

Substituting Eqs. (3) and (4) into Eq. (2) and applying the small-strain assumption yield an alternative form of Green-Lagrange strain tensor $\mathbf{E}$, i.e.,

$$\mathbf{E} = (g_1 - G_1)G_1\mathbf{G}^1 \otimes \mathbf{G}^1 \tag{5}$$

or

$$E_{11} = (g_1 - G_1)G_1 \tag{6}$$

Some relations are obtained in terms of $k_0$ and $k$ that are, respectively, the initial and deformed curvatures as

$$\mathbf{A}_2' = -k_0\frac{\mathbf{A}_1}{A_1} \qquad \mathbf{a}_2' = -k\frac{\mathbf{a}_1}{a_1} \tag{7}$$

where $A_1$ is the length of $\mathbf{A}_1$.

With the aid of Eq. (7) and the forms of $\mathbf{G}_1$ and $\mathbf{g}_1$ in [3], $E_{11}$ is explicitly expressed as

$$\begin{aligned} E_{11} &= \Gamma_{11} + TK_{11} \\ &= A_1(a_1 - A_1) + T\left(\frac{A_1}{a_1}\mathbf{a}_1.\mathbf{a}_2' - \mathbf{A}_1.\mathbf{A}_2'\right) \end{aligned} \tag{8}$$

where $\Gamma_{11}$ is the membrane strain and $K_{11}$ is the bending curvature.

The energy conjugate of the Green-Lagrange strain $E_{11}$ is the second Polar-Kirchoff stress $S^{11}$ that is specified in the covariant curvilinear coordinate system $\mathbf{G}_{\alpha} \otimes \mathbf{G}_{\beta}$ as

$$S^{11} = \bar{E}E_{11} \tag{9}$$

where $\bar{E} = E/(A_1)^4$. In addition, $E$ is Young's modulus of the material, while $\bar{E}$ is Young's modulus expressed in the covariant curvilinear coordinate system.

### 2.2. Principle of virtual work

The virtual work principle is written as

$$\delta\Pi_{int} - \delta\Pi_{ext} = 0 \tag{10}$$

where $\delta\Pi_{int}$ and $\delta\Pi_{ext}$ are, respectively, the internal virtual work and the external virtual work, given by

$$\delta\Pi_{int} = \int_V \delta E_{11}S^{11}dV = \int_0^l \delta\mathbf{\Gamma}^{\mathrm{T}}\mathbf{D}\mathbf{\Gamma}\,\mathrm{d}S \tag{11}$$

$$\begin{aligned} \delta\Pi_{ext} = \int_0^l \left(\delta\mathbf{u}_0^{\mathrm{T}}\mathbf{f} + \delta\theta m\right)\mathrm{d}S + \delta u_{0X}(0)F_X(0) + \\ \delta u_{0Y}(0)F_Y(0) + \delta u_{0X}(l)F_X(l) + \delta u_{0Y}(l)F_Y(l). \end{aligned} \tag{12}$$

Here, $l$ is the initial length of the beam element and

$$\mathbf{\Gamma} = [\Gamma_{11} \quad K_{11}]^{\mathrm{T}} \qquad \mathbf{D} = \begin{bmatrix} \bar{E}A & 0 \\ 0 & \bar{E}I \end{bmatrix}. \tag{13}$$

In addition, $\mathbf{u}_0 = [u_X \quad u_Y]^{\mathrm{T}}$ and $\theta$ are the displacements and rotation of the beam axis, respectively. Moreover, $\mathbf{f} = [f_X \quad f_Y]^{\mathrm{T}}$ and $m$ are, respectively, the distributed forces and distributed moment applied on the beam axis. In addition, $F_X(0)$ and $F_Y(0)$ are the concentrated forces applied at $S = 0$, while $F_X(l)$ and $F_Y(l)$ are the concentrated forces applied at $S = l$.

### 2.3. Discretization of the kinematic unknowns

In isogeometric Euler-Bernoulli beam elements, the translational displacements of control points are usually considered degrees of freedom (DOFs). In this study, the beam element is approximated using cubic rational Bézier curves [1], as shown in Fig 2. The displacement vector $\mathbf{U}$ is introduced as

$$\mathbf{U} = [u_{X1} \quad u_{Y1} \quad u_{X2} \quad u_{Y2} \quad u_{X3} \quad u_{Y3} \quad u_{X4} \quad u_{Y4}]^{\mathrm{T}} \tag{14}$$

where $u_{Xi}$ and $u_{Yi}$ are the displacements of control point $\mathbf{P}_i$ in $X$ and $Y$ directions.

Accordingly, the virtual work terms are written as

$$\delta\Pi_{int} = \delta\mathbf{U}^{\mathrm{T}}\int_0^l \mathbf{B}^{\mathrm{T}}\mathbf{D}\mathbf{\Gamma}dS \tag{15}$$

$$\delta\Pi_{ext} = \tag{16}$$



 

$$\delta\mathbf{U}^{\mathrm{T}}\int_0^l(\mathbf{H}_X^{\mathrm{T}}f_X+\mathbf{H}_Y^{\mathrm{T}}f_Y+\mathbf{H}_\theta^{\mathrm{T}}m)dS+\ \delta\mathbf{U}^{\mathrm{T}}\mathbf{F}.$$

Here,

$$\mathbf{B}=\begin{bmatrix}\mathbf{B}_{\Gamma_{11}}^{\mathrm{T}} & \mathbf{B}_{K_{11}}^{\mathrm{T}}\end{bmatrix}^{\mathrm{T}} \tag{17}$$

$$\mathbf{B}_{\Gamma_{11}}=$$

$$\begin{bmatrix}\frac{\partial\Gamma_{11}}{\partial x_1} & \frac{\partial\Gamma_{11}}{\partial y_1} & \frac{\partial\Gamma_{11}}{\partial x_2} & \frac{\partial\Gamma_{11}}{\partial y_2} & \frac{\partial\Gamma_{11}}{\partial x_3} & \frac{\partial\Gamma_{11}}{\partial y_3} & \frac{\partial\Gamma_{11}}{\partial x_4} & \frac{\partial\Gamma_{11}}{\partial y_4}\end{bmatrix} \tag{18}$$

$$\mathbf{B}_{K_{11}}=$$

$$\begin{bmatrix}\frac{\partial K_{11}}{\partial x_1} & \frac{\partial K_{11}}{\partial y_1} & \frac{\partial K_{11}}{\partial x_2} & \frac{\partial K_{11}}{\partial y_2} & \frac{\partial K_{11}}{\partial x_3} & \frac{\partial K_{11}}{\partial y_3} & \frac{\partial K_{11}}{\partial x_4} & \frac{\partial K_{11}}{\partial y_4}\end{bmatrix} \tag{19}$$

$$\mathbf{H}_X=$$

$$\begin{bmatrix}\frac{\partial u_X}{\partial x_1} & \frac{\partial u_X}{\partial y_1} & \frac{\partial u_X}{\partial x_2} & \frac{\partial u_X}{\partial y_2} & \frac{\partial u_X}{\partial x_3} & \frac{\partial u_X}{\partial y_3} & \frac{\partial u_X}{\partial x_4} & \frac{\partial u_X}{\partial y_4}\end{bmatrix} \tag{20}$$

$$\mathbf{H}_Y=$$

$$\begin{bmatrix}\frac{\partial u_Y}{\partial x_1} & \frac{\partial u_Y}{\partial y_1} & \frac{\partial u_Y}{\partial x_2} & \frac{\partial u_Y}{\partial y_2} & \frac{\partial u_Y}{\partial x_3} & \frac{\partial u_Y}{\partial y_3} & \frac{\partial u_Y}{\partial x_4} & \frac{\partial u_Y}{\partial y_4}\end{bmatrix} \tag{21}$$

$$\mathbf{H}_\theta=$$

$$-\frac{\mathbf{a}_1}{a_1}\cdot\begin{bmatrix}\frac{\partial\mathbf{a}_2}{\partial x_1} & \frac{\partial\mathbf{a}_2}{\partial y_1} & \frac{\partial\mathbf{a}_2}{\partial x_2} & \frac{\partial\mathbf{a}_2}{\partial y_2} & \frac{\partial\mathbf{a}_2}{\partial x_3} & \frac{\partial\mathbf{a}_2}{\partial y_3} & \frac{\partial\mathbf{a}_2}{\partial x_4} & \frac{\partial\mathbf{a}_2}{\partial y_4}\end{bmatrix}. \tag{22}$$

Moreover, **F** is the applied nodal force vector, written as

$$\mathbf{F}=$$

$$[F_X(0)\quad F_Y(0)\quad 0\quad 0\quad 0\quad 0\quad F_X(l)\quad F_Y(l)]^T. \tag{23}$$

Eventually, the equation system can be obtained by substituting Eqs. (15) and (16) into Eq. (10) as

$$\int_0^l\mathbf{B}^{\mathrm{T}}\mathbf{D}\boldsymbol{\Gamma}dS=\int_0^l\left(\mathbf{H}_X^{\mathrm{T}}f_X+\mathbf{H}_Y^{\mathrm{T}}f_Y+\mathbf{H}_\theta^{\mathrm{T}}m\right)dS+\mathbf{F}. \tag{24}$$

## 3. A DEEP CIRCULAR ARCH SUBJECTED TO A CONCENTRATED FORCE AT THE APEX

In this section, the proposed element is applied to analyze a deep circular arch subjected by a downward concentrated force $P$ at its apex $B$ as described in Fig 3. The arch has a pinned support at point $A$ and a clamped support at point $C$.

To appraise the efficiency and accuracy of the element, the displacements of the apex $B$ are investigated. The numerical solutions in [5] are adopted as references. To solve the problem, this study employs 24 proposed elements with 73 control points or 118 DOFs. The load-displacement curves obtained in this work are plotted together with the reference solutions in Fig 4. In the figure, $u_X$ is the displacement in $X$ direction and $u_Y$ is the displacement in $Y$ direction. Moreover, $E$ is Young's modulus of the material while $I$ is the in-plane cross-sectional moment of inertia.

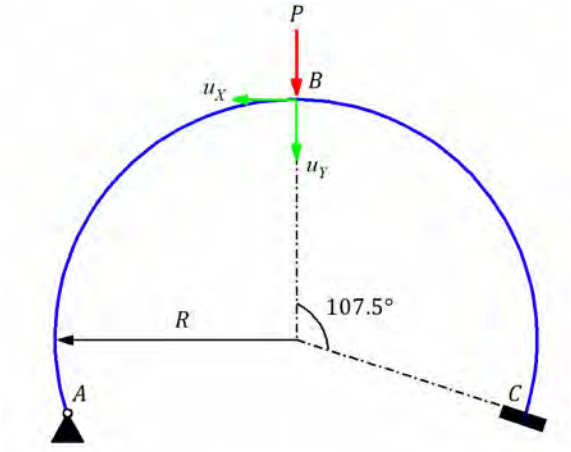


Fig 3. A deep circular arch

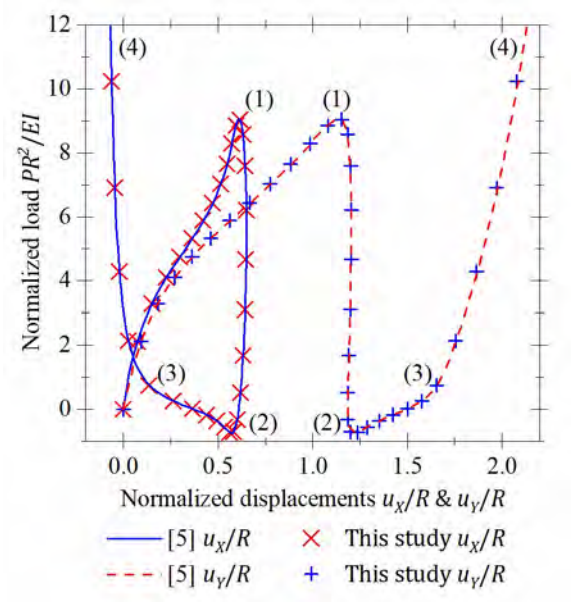


Fig 4. Normalized load-displacement curves of the apex

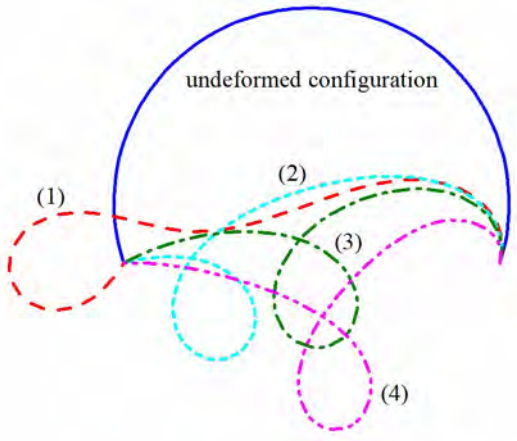


Fig 5. Initial configuration and deformed configurations of the arch at the snap points

The numerical solutions give good agreement with the reference ones. The arch exhibits severe snap points, i.e., snap-through and snap-back points. These snap points require the problem to be solved by the displacement control method [6]. The deformed configurations at the snap points (1), (2), (3), and (4) are illustrated in Fig 5. This problem is also investigated in other studies, e.g., in [7], where the arch is simulated by 20 three-noded curved beam elements with 123 DOFs.

## 4. CONCLUSIONS AND REMARKS

A curved Euler-Bernoulli beam element for analysis of curved beams undergoing large displacements and small strains is developed using the total Lagrangian description. Isogeometric representations using rational cubic Bézier curves are employed to approximate the element and discretize the kinematic unknowns. The validity of the proposed element is demonstrated by analyzing a deep circular arch subjected to a concentrated force at its apex. Under the load, the arch exhibits severe snap-through and snap-back behavior; therefore, the displacement control method is required for the analysis.

Due to the use of a curvilinear coordinate system and the isogeometric approach, the element exhibits flexibility in solving problems with complex geometry and large displacements. Concretely, the accuracy of the element is proved by the obtained good numerical results. Furthermore, being able to solve a problem with snap behavior strongly displays the reliability and efficiency of the formulation derived.

## ACKNOWLEDGMENTS

Scholarships, under the Collaborative Education Program (CEP), from the ASEAN University Network/Southeast Asia Engineering Education Development Network (AUN/SEED-Net), Sirindhorn International Institute of Technology (SIIT) of Thammasat University, and the Graduate School of Engineering of Hokkaido University for the first author are greatly appreciated.

## REFERENCES

1. Vo, D., et al., A 2D field-consistent beam element for large displacement analysis using a rational Bézier representation with varying weights. Applied Mathematical Modelling, 2021.
2. Chorn, V., D. Vo, and P. Nanakorn, A Total Lagrangian Isogeometric Timoshenko Beam Formulation for Large Displacement Analysis of 2D Frames, in EASEC16. 2021, Springer. p. 961-968.
3. Vo, D. and P. Nanakorn, Geometrically nonlinear multi-patch isogeometric analysis of planar curved Euler–Bernoulli beams. Computer Methods in Applied Mechanics and Engineering, 2020. 366: p. 113078.
4. Vo, D. and P. Nanakorn, A total Lagrangian Timoshenko beam formulation for geometrically nonlinear isogeometric analysis of planar curved beams. Acta Mechanica, 2020. 231(7): p. 2827-2847.
5. Zhong, J. and S.D. Ross, Differential correction and arc-length continuation applied to boundary value problems: Examples based on snap-through of circular arches. Applied Mathematical Modelling, 2021. 97: p. 81-95.
6. Torkamani, M.A. and M. Sonmez. Solution techniques for nonlinear equilibrium equations. in Structures Congress 2008: 18th Analysis and Computation Specialty Conference. 2008.
7. Ibrahimbegović, A., On finite element implementation of geometrically nonlinear Reissner's beam theory: three-dimensional curved beam elements. Computer methods in applied mechanics and engineering, 1995. 122(1-2): p. 11-26.



 